Decreased mechanotransduction prevents nuclear collapse in a *Caenorhabditis elegans* laminopathy

Gabriela Huelgas-Morales[a], Mark Sanders[b], Gemechu Mekonnen[a], Tatsuya Tsukamoto[a], and David Greenstein[a,1]

[a]Department of Genetics, Cell Biology, and Development, University of Minnesota, Minneapolis, MN 55455; and [b]University Imaging Center, University of Minnesota, Minneapolis, MN 55455

Edited by Iva Greenwald, Columbia University, New York, NY, and approved October 28, 2020 (received for review July 20, 2020)

The function of the nucleus depends on the integrity of the nuclear lamina, an intermediate filament network associated with the linker of nucleoskeleton and cytoskeleton (LINC) complex. The LINC complex spans the nuclear envelope and mediates nuclear mechanotransduction, the process by which mechanical signals and forces are transmitted across the nuclear envelope. In turn, the AAA+ ATPase torsinA is thought to regulate force transmission from the cytoskeleton to the nucleus. In humans, mutations affecting nuclear envelope-associated proteins cause laminopathies, including progeria, myopathy, and dystonia, though the extent to which endogenous mechanical stresses contribute to these pathologies is unclear. Here, we use the *Caenorhabditis elegans* germline as a model to investigate mechanisms that maintain nuclear integrity as germ cell nuclei progress through meiotic development and migrate for gametogenesis—processes that require LINC complex function. We report that decreasing the function of the *C. elegans* torsinA homolog, OOC-5, rescues the sterility and premature aging caused by a null mutation in the single worm lamin homolog. We show that decreasing OOC-5/torsinA activity prevents nuclear collapse in lamin mutants by disrupting the function of the LINC complex. At a mechanistic level, OOC-5/torsinA promotes the assembly or maintenance of the lamin-associated LINC complex and this activity is also important for interphase nuclear pore complex insertion into growing germline nuclei. These results demonstrate that LINC complex-transmitted forces damage nuclei with a compromised nuclear lamina. Thus, the torsinA–LINC complex nexus might comprise a therapeutic target for certain laminopathies by preventing damage from endogenous cellular forces.

nuclear lamina | torsinA | nuclear mechanotransduction | laminopathy | LINC complex

Nuclear mechanotransduction enables the nucleus to adapt its rigidity in response to applied forces and is necessary for transmitting mechanical signals across the nuclear envelope (NE) and for maintaining the integrity of the genome (1, 2). Nuclear mechanotransduction requires an intact nuclear lamina, which comprises an intermediate filament network of lamins and associated proteins that line the nuclear-facing surface of the NE. The LINC (linker of nucleoskeleton and cytoskeleton) complex is a core NE component required for nuclear mechanotransduction, as it acts as a molecular bridge coupling the inside of the nucleus with the cytoplasm. The LINC complex consists of two interacting protein components: 1) SUN (Sad1 and UNC-84) domain proteins in the inner nuclear membrane; and 2) KASH (Klarsicht, ANC-1, Syne homology) domain proteins in the outer nuclear membrane (2). The LINC complex is tethered to the cytoplasmic cytoskeleton and nuclear lamins and transduces forces across the NE.

Mutations in many NE components are associated with a range of seemingly unrelated tissue-specific pathologies, collectively known as nuclear envelopathies (3). The apparent tissue specificity of these diseases is somewhat surprising because most of these NE components are widely expressed proteins. For example, mutations in genes encoding nuclear lamins cause diseases, including Hutchinson-Gilford progeria, dyslipidemias, and myopathies (3). By contrast, mutations affecting the NE-associated AAA+ ATPase (ATPases associated with diverse cellular activities) torsinA cause early-onset DYT1 dystonia and congenital joint contractures (4–6). An attractive hypothesis is that endogenous mechanical forces contribute to the pathology of nuclear envelopathies by causing damage to cells with defective NE components, yet few studies have directly tested this possibility. In many cases, experimental investigations are hampered by the fact that the mechanistic functions of many key NE components remain incompletely understood—such is the case of torsinA.

In this study, we set out to elucidate molecular interactions and mechanisms by which torsinA functions in the NE. Although the cellular functions of torsinA have remained enigmatic, they appear to be conserved across cell types and species because distantly related organisms lacking torsinA function display similar ultrastructural NE defects (7, 8). A plausible hypothesis is that torsinA plays a role in regulating nuclear mechanotransduction, as its loss disrupts cell migration, nuclear positioning, and polarization (8–10). Yet, torsinA has been implicated in other cellular processes, including endoplasmic reticulum (ER) stress (11–14), lipid metabolism (15), and membrane remodeling (16). In this study, we took advantage of the fact that mutations in the *Caenorhabditis elegans* torsinA ortholog, OOC-5 (abnormal oocyte formation, 5), cause oocyte growth and embryonic polarity defects

Significance

Nuclear envelopathies are a complex group of human diseases caused by mutations in nuclear envelope proteins, including progeria, myopathy, and dystonia. Here, we used the *Caenorhabditis elegans* germline as a model system to investigate the function of the OOC-5/torsinA AAA+ ATPase, which localizes to the nuclear envelope and is mutated in early-onset DYT1 dystonia in humans. We show that OOC-5/torsinA promotes the function of the LINC complex, which spans the nuclear envelope and transmits forces to the nuclear lamina. Remarkably, decreasing the function of OOC-5/torsinA or the LINC complex prevents nuclear collapse in the absence of a functional nuclear lamina. Therapeutics targeting torsinA or the LINC complex might prevent nuclear damage from endogenous forces in certain nuclear envelopathies.

Author contributions: G.H.-M. and D.G. designed research; G.H.-M., M.S., G.M., T.T., and D.G. performed research; G.H.-M., M.S., G.M., T.T., and D.G. contributed new reagents/analytic tools; G.H.-M., M.S., G.M., and D.G. analyzed data; and G.H.-M. and D.G. wrote the paper.

The authors declare no competing interest.

This article is a PNAS Direct Submission.

[1]To whom correspondence may be addressed. Email: green959@umn.edu.

This article contains supporting information online at https://www.pnas.org/lookup/suppl/doi:10.1073/pnas.2015050117/-/DCSupplemental.

First published November 23, 2020.

(17, 18). Further, we used the *C. elegans* germline as a model system to investigate how cytoskeletal forces are transduced as germ cell nuclei progress through meiosis and migrate for gametogenesis. Our results reveal that OOC-5/torsinA promotes the activity of the LINC complex in transducing forces to the nuclear lamina. Remarkably, decreasing the function of OOC-5/torsinA or the LINC complex prevents nuclear collapse in the absence of a functional nuclear lamina. These results highlight a critical role for torsinA in nuclear mechanotransduction and suggest that an inability to cope with endogenous and exogenous forces may underlie the etiology of nuclear envelopathies.

Results

OOC-5/TorsinA Associates with the LINC Complex Protein SUN-1 and Lamin. To address the mechanism of OOC-5 function, we purified OOC-5-associated proteins from soluble and membrane protein fractions using tandem affinity purification (*SI Appendix*, Fig. S1). Both purifications identified highly conserved regulators of ER and NE homeostasis (*SI Appendix*, Table S1). The OOC-5-associated proteins include OOC-3, a protein required for OOC-5 localization and function (17, 18), ER chaperone CNX-1/calnexin, which associates with torsinA in mammalian cells (19), and GEI-18 and T09B4.2, the divergent *C. elegans* homologs of the torsinA-interacting proteins LAP1 and LULL1 (20).

Also, among the OOC-5-associated proteins was SUN-1, the SUN domain inner nuclear membrane protein component of LINC complexes in the *C. elegans* germline (21). SUN domain proteins interact with nuclear lamins (22, 23), and the sole *C. elegans* lamin, LMN-1 (24), was well represented among OOC-5-associated proteins (42 to 43% protein coverage; *SI Appendix*, Table S1). The genetic interaction studies described below suggest that the association between OOC-5, which resides in the lumen of the NE and ER, and nucleoplasmic LMN-1 is likely mediated through SUN-1.

Decreasing OOC-5/TorsinA Function Prevents Nuclear Collapse and Extends Lifespan in Lamin Mutants. To address the significance of the protein associations with OOC-5, we conducted genetic analyses. The most striking result was an interaction between *ooc-5* and *lmn-1*. Most *lmn-1* null mutants are agametic, sterile, and have small gonads (Figs. 1*A* and 2*A*). However, 12.3 ± 7.8% of animals ("escapers") develop larger gonads and produce dead embryos (Figs. 1*A* and 2*A*). Surprisingly, compromising *ooc-5* function rescued the sterility of *lmn-1* mutants such that all animals produced gametes and dead embryos (Figs. 1*A* and 2*A* and *SI Appendix*, Fig. S2*A*). Importantly, reducing the dosage of *ooc-5* was sufficient to suppress *lmn-1* sterility (Figs. 1*A* and 2*A*). These and the following genetic analyses were performed using a deletion of the *ooc-5* locus that we generated by CRISPR-Cas9 genome editing (*SI Appendix*, Fig. S1*A*). Yet, similar results were observed for other *ooc-5* alleles ($n = 69$ for the *tn1709* deletion allele, and $n = 57$ for the *it145* R95stop nonsense allele). Because prior work established that *lmn-1(–)* mutants exhibit a reduced lifespan (25), we tested whether decreasing *ooc-5* function could suppress the premature aging observed in *lmn-1(–)* mutants. Indeed, reducing or eliminating *ooc-5* function suppressed the decreased lifespan of *lmn-1(–)* mutants (Fig. 1*B* and *SI Appendix*, Table S2). Importantly, reducing or eliminating *ooc-5* function did not increase lifespan in an otherwise wild-type genetic background (Fig. 1*B* and *SI Appendix*, Table S2).

The germ cells of the *lmn-1* escapers appeared to deteriorate as they progressed through meiotic prophase; they assembled a synaptonemal complex (SC) but their nuclei appeared to collapse soon after the pachytene stage (*SI Appendix*, Figs. S3*D* and S4). We assessed the dynamic nature of this apparent nuclear collapse using time-lapse imaging of *lmn-1* mutant gonads (Fig. 1*C* and Movies S1–S3). Proximal germ cell nuclei that appeared normal in size and shape at the beginning of the recording were observed to rapidly condense and even fragment. We observed nuclear collapse in *lmn-1(–)* mutants in at least three situations: 1) simultaneously with the ovulation of the most proximal oocyte (Fig. 1 *C*, *Top* and Movie S1); 2) spontaneously in a cellularized oocyte (Fig. 1 *C*, *Middle* and Movie S2); and 3) while migrating in the proximal direction with the cytoplasmic flows, which also resulted in nuclear fragmentation (Fig. 1 *C*, *Bottom* and Movie S3). In all cases, nuclear collapse occurred within the span of a few minutes. We also observed that SUN-1 lost its normal NE localization and appeared diffuse in most collapsing nuclei (*SI Appendix*, Fig. S5 *C* and *D*). Remarkably, reducing the dosage of *ooc-5* prevented the nuclear collapse in lamin mutants (Fig. 1*A* and *SI Appendix*, Fig. S3*C*). Whereas diakinesis-stage chromosomes were rare in *lmn-1* mutant oocytes, they were observed in most or all *lmn-1* mutants after reducing *ooc-5* function (Fig. 1*A* and *SI Appendix*, Fig. S3*C*). Further, reducing or eliminating *ooc-5* function enabled SUN-1 to retain its NE association in *lmn-1* mutants (*SI Appendix*, Fig. S5 *E* and *F*). Additionally, we observed increased levels of DNA damage in late-stage pachytene female germ cells of *lmn-1* mutants (*SI Appendix*, Fig. S6). Nevertheless, decreasing *ooc-5* function did not appear to completely rescue this defect (*SI Appendix*, Fig. S6 *A* and *B*).

OOC-5/TorsinA Acts through the LINC Complex. Studies in mammalian cells suggest that torsinA regulates force transmission from the cytoplasm to the nucleus (9, 10). Thus, we examined a model in which OOC-5 promotes LINC complex function, which damages nuclei with a compromised nuclear lamina. We tested for genetic interactions between *lmn-1(–)* mutants and genes encoding components of the LINC complex, utilizing mutations in *sun-1* and *zyg-12*, which encodes the KASH domain outer nuclear membrane LINC complex component in the germline (21). As observed for *ooc-5*, the proportion of fertile *lmn-1(–)* mutant animals increased when LINC complex function was compromised, and nuclear collapse was substantially ameliorated (Fig. 2*A* and *SI Appendix*, Fig. S2*B*). These results suggest that OOC-5 and LINC complex-transmitted forces contribute to nuclear damage in *lmn-1* mutants.

OOC-5/TorsinA Promotes LINC Assembly or Maintenance in Growing Late Prophase Meiotic Nuclei. TorsinA function is required for the proper localization of KASH domain proteins ZYG-12 and nesprin3 in *C. elegans* germ cells and mammalian fibroblasts, respectively (8, 9). To assess whether OOC-5 promotes LINC complex integrity, we used superresolution microscopy to examine the colocalization of SUN-1 and ZYG-12 in the wild type and *ooc-5* mutants. Prior work showed discontinuities in ZYG-12 localization in *ooc-5* mutants commencing in pachytene germ cells (8). In addition to these discontinuities, we observed a reduction of ZYG-12 NE localization as germ cells progressed from the pachytene stage to the diakinesis stage of meiotic prophase (Fig. 2*B*). By contrast, SUN-1 remained in the NE at high levels in *ooc-5* mutants (Fig. 2*B*). We quantified SUN-1 and ZYG-12 colocalization as a function of nuclear diameter by measuring Pearson's correlation and Mander's overlap as a function of nuclear diameter. We observed that as the *ooc-5(–)* germ cells grew, colocalization declined (Fig. 2*C*). These results suggest that OOC-5 promotes the assembly or maintenance of the LINC complex, which appears particularly important for growing meiotic prophase nuclei.

OOC-5/TorsinA Promotes the Activity of the LINC Complex in Early Meiotic Prophase Nuclei. The LINC complex is essential for the pairing of homologous chromosomes in *C. elegans* meiosis (26–28). OOC-5 is not required for SC formation (*SI Appendix*, Figs. S3*B* and S4) and appears dispensable for meiotic chromosome segregation (17, 18). To examine whether OOC-5 promotes

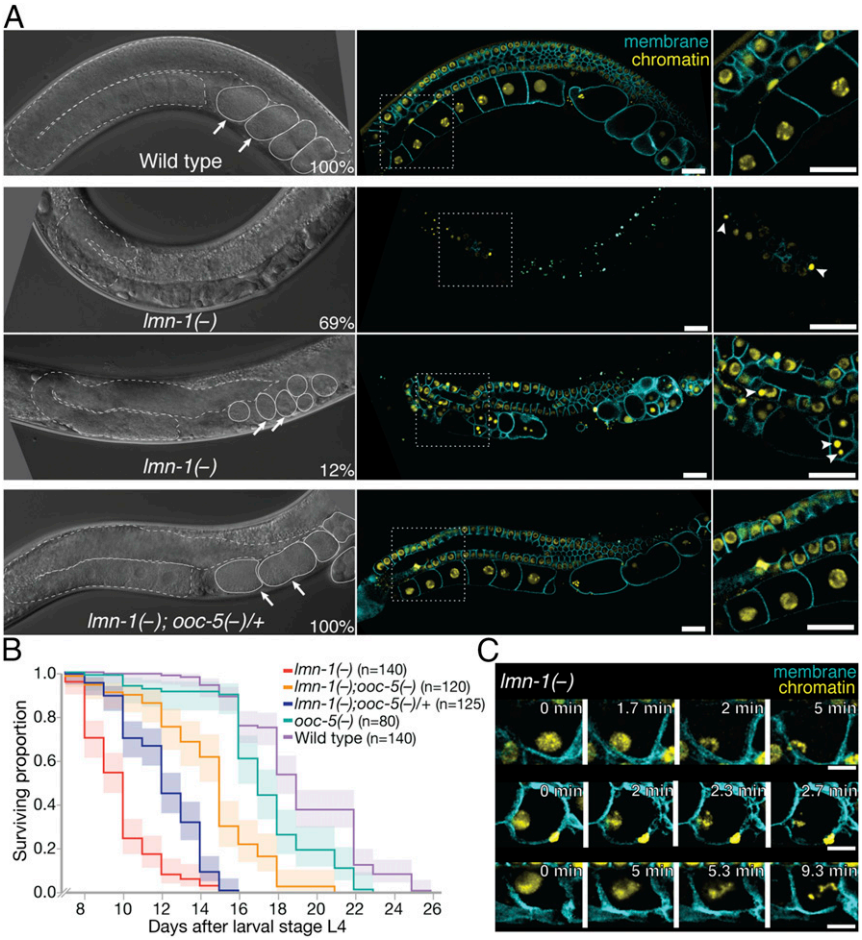

Fig. 1. Loss of *ooc-5* rescues defects in lamin mutants. (*A*) Differential interference contrast and fluorescence micrographs of adult hermaphrodites. Cellular membranes of germ cells are visualized using a GFP::PH domain fusion and chromatin is visualized with a histone H2B::mCherry fusion. *Insets* are twice the size of the dotted-line region. Arrows indicate embryos and arrowheads indicate collapsing nuclei. (Scale bars, 20 μm.) (*B*) Kaplan-Meier survival curves of the indicated genotypes. Three replicates were conducted, and confidence intervals are shadowed. (*C*) Time-lapse imaging of three instances of nuclear collapse in proximal oocytes of different *lmn-1(–)* escaper animals (Movies S1–S3). (Scale bars, 10 μm.) Alleles used: *tm1502* as *lmn-1(–)* and *tn1757* as *ooc-5(–)*. *itIs37* [*pie-1p::mCherry::H2B::pie-1* 3′ UTR] was used to mark chromatin and *itIs38*[*pie-1p::GFP::PH(PLC1delta1)*] was used to mark the plasma membrane in C. The *mIn1* balancer chromosome was used to analyze the *ooc-5(–)/+* genotype.

the efficiency of meiotic pairing, we examined the localization of ZIM-3 and HIM-8, which bind the pairing center regions on chromosomes I and IV and the X chromosome, respectively (29). The spatial distribution of unpaired meiotic chromosomes across the distal gonad suggests that pairing of chromosomes I and IV is delayed in *ooc-5* mutants (Fig. 3 *A* and *B*, *Upper*). By contrast, *ooc-5* appears dispensable for the timely pairing of the X chromosome (Fig. 3 *A* and *B*, *Lower*). Persistent SUN-1 phosphorylation correlates with synaptic or recombination defects (30). We observed that phosphorylated SUN-1 (S8Pi) persisted in an extended zone in *ooc-5* mutants (Fig. 3 *C* and *D*), and that the number of SUN-1 foci and their speed of motion increased (Fig. 3 *E* and *F* and Movies S4–S6). The increased movement of SUN-1 foci in *ooc-5* mutants may reflect a partial release from cytoskeletal tension. By contrast, we observed lower numbers and slower movement of SUN-1 foci in *lmn-1* mutants (Fig. 3 *E* and *F*). We hypothesize that this observation reflects a lower level of force resistance exerted by the weakened nuclear lamina in the absence of LMN-1 such that the SUN-1 foci are subjected to enhanced cytoskeletal tension and thus move more slowly and coalesce into fewer foci. Taken together, these results suggest that the function of the LINC complex is perturbed in *ooc-5* mutants even in early prophase germ cells, which exhibit normal SUN-1 and ZYG-12 colocalization.

OOC-5/TorsinA and the LINC Complex Promote Interphase Nuclear Pore Insertion. *C. elegans* OOC-5 and mammalian torsinA are required for the proper localization of nuclear pore complex (NPC) proteins (8, 31). Mislocalization of nucleoporins (Nups) may be sufficient to explain the embryonic polarity defects in *ooc-5* mutants (32). The two transmembrane Nups, NPP-12 and NPP-22, were identified among OOC-5-associated proteins (*SI Appendix*, Table S1). A prior study concluded that an NPP-22::GFP-expressing transgene localized more normally in *ooc-5* mutants than other Nups, but the localization of NPP-12 was not examined (8). Thus, we used genome editing to generate GFP fusions to the endogenous transmembrane Nups and analyzed their localization. By examining the localization of these two fusion proteins we confirmed that they localize to patches within the NE of *ooc-5* mutant germ cells, consistent with the previous report (8). However, we observed further localization changes in that both NPP-12::GFP and GFP::NPP-22 exhibited substantial mislocalization in *ooc-5* mutants, accumulating largely outside the NE and in the cytoplasm of proximal oocytes (Fig. 4 *A* and *B*). We tested the possibility that this mislocalization of transmembrane Nups in *ooc-5* mutants might be a consequence of the impaired function of the LINC complex. Thus, we used a temperature-sensitive *zyg-12* mutant allele to examine the localization of

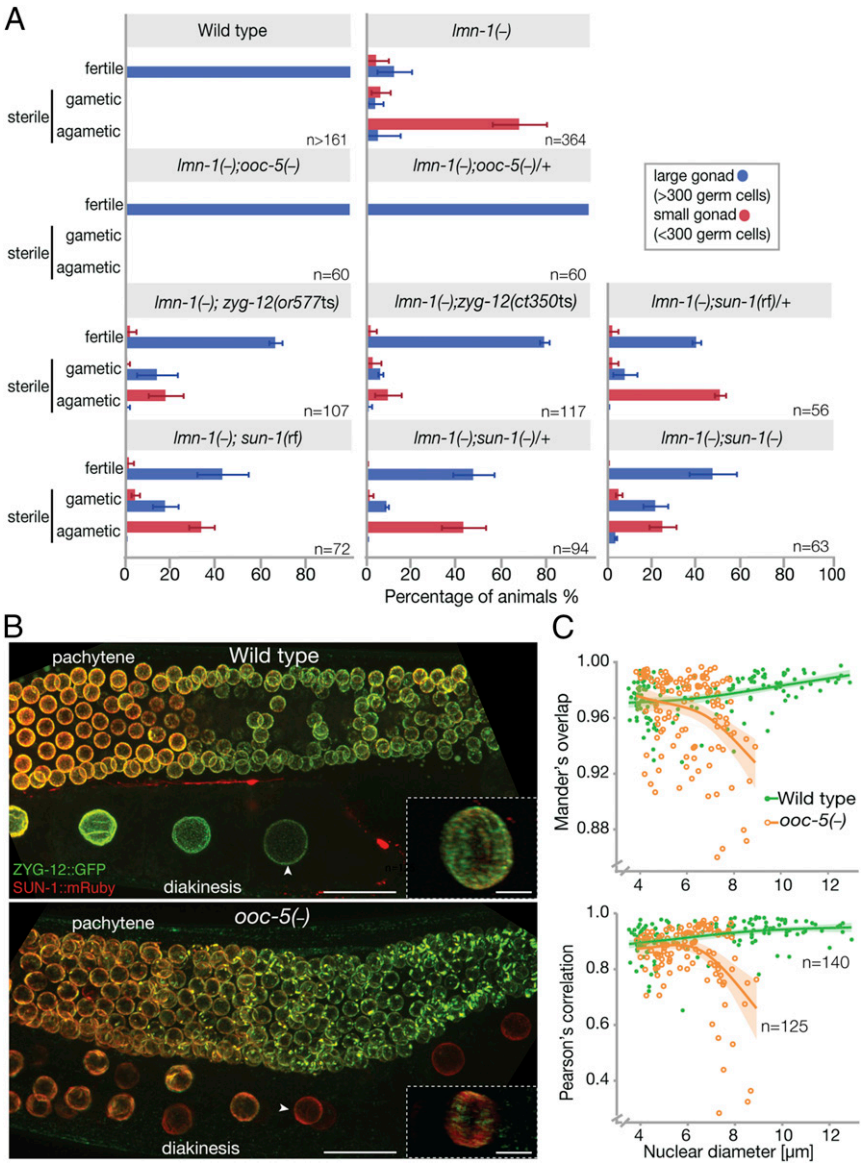

Fig. 2. OOC-5 regulates the LINC complex. (*A*) Hermaphrodites of the indicated genotypes grown at 20 °C, were classified as fertile (≥1 embryo), sterile gametic (sperm/oocytes), or sterile agametic. Animals with more than 300 germ cells in a gonad arm were further classified as having large (blue) versus small gonads (red). Alleles used: *tm1502 as lmn-1(–), tn1757* as *ooc-5(–), jf18* as *sun-1*(rf), and *gk199* as *sun-1(–)*. The balancers used to analyze the heterozygous genotypes are listed in *SI Appendix*, Table S3. (*B*) Maximum projections of Z-stack superresolution confocal images of ZYG-12::GFP and SUN-1::mRuby in the gonad. (Scale bars, 20 μm.) *Insets* are magnified three-dimensional reconstructions of the nuclei indicated with arrowheads. (Scale bars, 5 μm.) (*C*) Colocalization of ZYG-12::GFP and SUN-1::mRuby in the NE. Bootstrap confidence regions are shadowed.

NPP-12::GFP and GFP::NPP-22 at the restrictive temperature. We observed that both NPP-12::GFP and GPF::NPP-22 exhibited clear mislocalization in the germlines *zyg-12* mutants (Fig. 4 *A* and *B*). We also examined the effect of a *sun-1* reduction-of-function (rf) allele on the localization of these transmembrane Nups. We found that NPP-12::GFP and GFP::NPP-22 abnormally aggregate in a patchy pattern on the NE of *sun-1*(rf) nuclei, but they only subtly changed their subcellular localization (Fig. 4 *A* and *B*). The subtle effect on the localization of Nups might be a reflection of the reduction-of-function nature of this *sun-1* allele.

Discussion

Decreased function of torsinA, the LINC complex, lamins, and other NE-associated proteins, result in altered nuclear deformability (1, 2, 33). Prior studies suggest that torsinA might function as a regulator of the LINC complex (9, 10). Four of our findings provide direct support for this model: 1) OOC-5 associates with SUN-1, as detected using tandem affinity purification (*SI Appendix*, Table S1); 2) mutations in OOC-5 and LINC complex components can suppress nuclear collapse in lamin null mutants (Fig. 2*A*); 3) OOC-5 is required for LINC complex assembly or maintenance in growing oocyte nuclei (Fig. 2 *B* and *C*); and 4) LINC complex-dependent activities, including the pairing of meiotic chromosomes and interphase nuclear pore insertion, are misregulated in the germline of *ooc-5* mutants (Figs. 3 and 4 and Movies S4–S6). Consistent with these findings, observations in mouse embryos suggest that torsinA acts upstream of the LINC complex (34). However, decreasing the dosage of the LINC complex protein Sun2 prevented abnormal brain morphogenesis in torsinA-deficient mouse embryos (34). Taken together with our results, this latter finding suggests that torsinA might promote or inhibit LINC complex-dependent activities depending

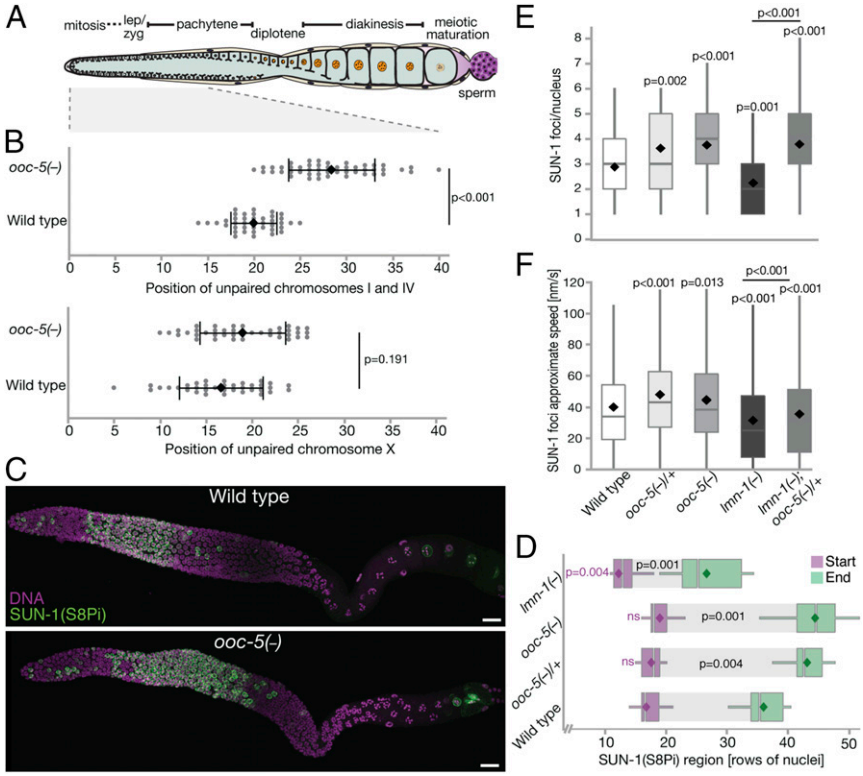

Fig. 3. LINC complex function during meiosis is compromised in *ooc-5* mutants. (*A*) Diagram of the *C. elegans* adult hermaphrodite gonad. (*B*) Spatial distribution of unpaired chromosomes I and IV, and X chromosomes, visualized by immunostaining for ZIM-3 and HIM-8, respectively (*SI Appendix*, Fig. S7 *A–D*). (*C*) Gonads immunostained for phosphorylated SUN-1 (S8Pi, green) and DNA (magenta). (Scale bars, 20 μm.) (*D*) Extent of the meiotic region containing phosphorylated SUN-1 (S8Pi). The rows of nuclei from start (magenta) to end (green) for the SUN-1 (S8Pi) region are specified. Diamonds indicate mean values. The statistical analyses for the start rows (magenta) and for the extent of the region (black) is depicted. (*E* and *F*) Quantification of SUN-1 foci per nucleus and their approximate speed of movement from time-lapse images (Movies S4–S6). Alleles used: *tm1502* as *lmn-1(–)* and *tn1757* as *ooc-5(–)*. The *mIn1* balancer chromosome was used to analyze the *ooc-5(–)/+* genotype.

on cellular context or the specific SUN-KASH pairs composing the particular LINC complexes. Further work will be needed to determine the precise molecular mechanisms by which torsinA regulates the activity of LINC complexes.

When torsinA is not functional, cells accumulate abnormal vesicles within the perinuclear space, which are often referred to as "blebs" (7, 8, 35, 36). One possibility is that the NE blebs observed in torsinA mutant cells might originate from defects in interphase NPC assembly or insertion. Consistent with this possibility, budding yeast mutants that disrupt the process of NPC insertion or assembly accumulate similar NE blebs (37, 38). In multiple cell types lacking torsinA function, several Nups localize to abnormal perinuclear plaque-like structures (8, 31). In this study, we found that OOC-5/torsinA associates with the two *C. elegans* transmembrane Nups, NPP-12 and NPP-22, and that these proteins lose their strict NE localization in the growing nuclei of *ooc-5* mutant oocytes (Fig. 4 *A* and *B* and *SI Appendix*, Table S1). The mislocalization of transmembrane Nups in *ooc-5* mutants might be a consequence of the impaired function of the LINC complex because NPP-12::GFP and GFP::NPP-22 were mislocalized in *sun-1* and *zyg-12* mutants (Fig. 4 *A* and *B*). In support of this idea, prior work found that Sun1 disruption in mammalian cells leads to NPC mislocalization (39).

The physical association between the LINC complex and nuclear lamins is critical for nuclei to prevent deformation under mechanical stress (1, 2). Our findings suggest that in the absence of a functional nuclear lamina, LINC complex-dependent forces, promoted by OOC-5, result in nuclear damage (Fig. 4*C*). Using time-lapse microscopy, we were able to directly observe rapid nuclear collapse occurring in oocyte nuclei in the absence of LMN-1 (Movies S1–S3). Our work here capitalized on the fact that *C. elegans* has but a single nuclear lamin. Nonetheless, we speculate that rapid nuclear collapse might contribute to the pathology of laminopathies caused by milder perturbations to the nuclear lamina. Consistent with our model derived from studies of the *C. elegans* germline (Fig. 4*C*), disruptions of the LINC complex can ameliorate defects in cultured cells, mouse models of laminopathies, and fibroblasts derived from Hutchinson-Gilford progeria patients (40, 41). Age-related alterations in the ability to cope with mechanotransduction across the NE may contribute to progeroid syndromes and reduce normal healthspan.

Nuclear envelopathies exhibit a broad range of symptoms and are characterized by a complex pathophysiology. Understanding the normal cellular functions and interactions of NE components and how their function is perturbed in nuclear envelopathies is vital for advancing treatments. This study in the *C. elegans* germline system provides insights into the normal functions and interactions of torsinA with conserved NE components and elucidates how this normal function becomes deleterious when the structure of the nuclear lamina is compromised. Our findings indicate that OOC-5/torsinA promotes or modulates vital LINC complex functions needed for maintaining NE homeostasis. This activity of torsinA might be relevant to the pathophysiology of DYT1 dystonia because Sun1 deficiency leads to cerebellar ataxia in mice (42). Thus torsinA-dependent LINC complex activities might influence the pathophysiology of multiple nuclear envelopathies.

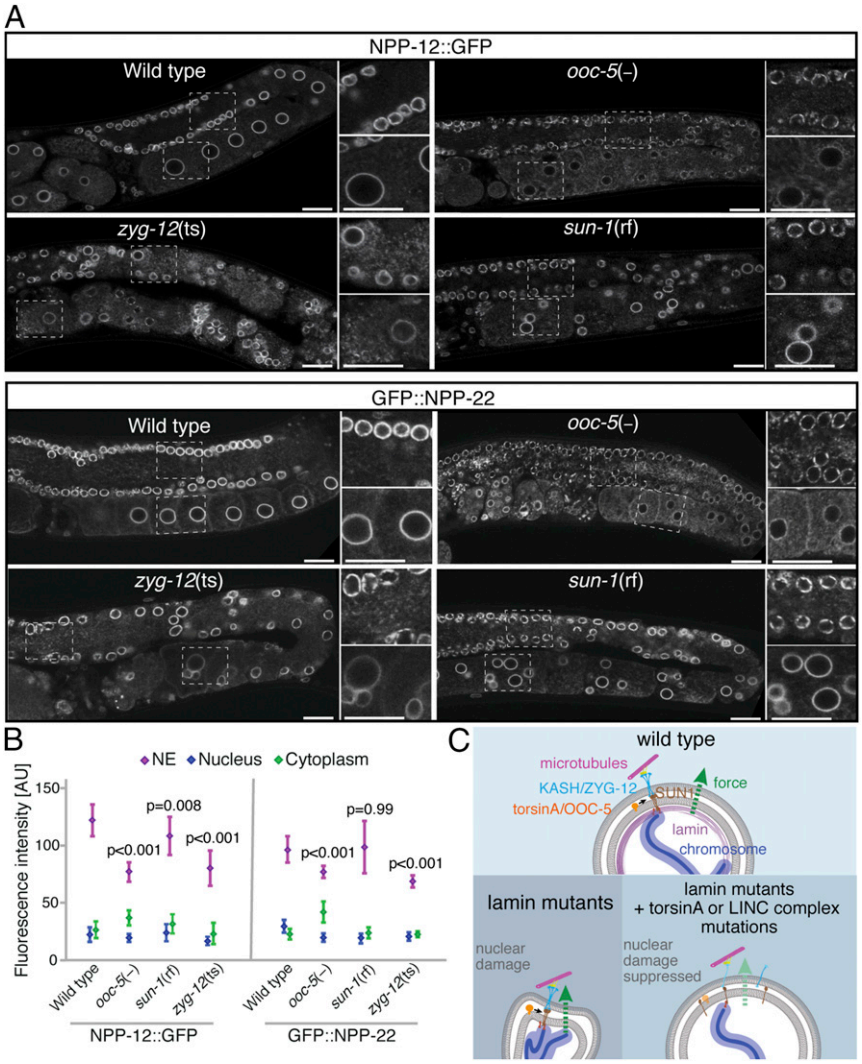

Fig. 4. OOC-5 and the LINC complex promote the localization of transmembrane Nups. (*A*) Confocal images of the expression of GFP::NPP-22 or NPP-12::GFP in the gonad. Animals were grown at 20 °C except *zyg-12*(ts) mutants, which were grown at 25 °C. (Scale bars, 20 μm.) (*B*) Quantification of the fluorescence intensity of GFP::NPP-22 or NPP-12::GFP in subcellular compartments of proximal oocytes (mean ± SD). Alleles used: *tn1757* as *ooc-5(–)*, *jf18* as *sun-1*(rf), and *ct350* as *zyg-12*(ts). (*C*) Model. OOC-5 promotes LINC complex function, which damages nuclei with a compromised nuclear lamina.

Materials and Methods

Detailed materials and methods are available in *SI Appendix, Materials and Methods*.

Strains. *C. elegans* strains were maintained at 20 °C on Nematode Growth Medium (NGM) and fed with the *Escherichia coli* strain OP50-1, unless otherwise noted (for the genotypes of all strains used see *SI Appendix*, Table S3). Genes and mutations are described in WormBase (https://wormbase.org/). The following mutations were used: LGI—*lmn-1(tm1502)*, *npp-12(tn1780 [npp-12::gfp::tev::3x-flag])*; LGII—*ooc-5(tn1757)*, *ooc-5(it145) unc-4(e120)*, *ooc-5(tn1709)*, *ooc-5(tn1758 [ooc-5::gfp::tev::3xflag])*, *zyg-12(or577*ts*)*, *zyg-12(ct350*ts*)*; and LGV—*sun-1(jf18)*, *sun-1(gk199)*, *npp-22(tn1794[gfp::tev::3xflag::npp-22])*. The following rearrangements were used: *tmC18[dpy-5(tmIs1236)]* I, *mIn1[dpy-10(e128)mIs14]* II, and *tmC12[egl-9(tmIs1194)]* V. The following transgenes and transgene insertions were used: *ieSi21[sun-1p::sun-1::mruby::sun-13′UTR + Cbr-unc-119]* IV, *itIs37[pie-1p::mCherry::H2B::pie-1 3′UTR + unc-119(+)]* IV, *ojIs9[zyg-12::gfp + unc-119(+)]*, and *itIs38[pie-1p::GFP::PH(PLC1delta1) + unc-119(+)]*. Phenotypic analyses were performed on well fed animals to avoid the effects of starvation in germline development.

Genome Editing. CRISPR-Cas9 genome editing used standard methods (43–46) as described in detail in *SI Appendix*. All new alleles were verified by Sanger sequencing and outcrossed to wild-type males at least three times. The sequence of oligonucleotides used to construct single-guide RNAs, repair templates, and sequencing primers are listed in Dataset S1.

OOC-5 Immunopurifications. OOC-5::GFP::TEV::3×FLAG and interacting proteins were purified from soluble protein extracts and membrane protein fractions prepared from the DG4377 strain using modifications of methods we previously described (47–49) as detailed in *SI Appendix*. Purifications from the wild-type strain (N2) were run in parallel as a control. Small aliquots of protein fractions from every step of the purifications were analyzed by Western blotting (Fig. 1*F* and *SI Appendix, Materials and Methods*).

Mass Spectrometry. Immunopurified proteins were concentrated on a centrifugal evaporator (Jouan RC 10-10 Vacuum Concentrator) for 5 h, briefly separated on a 12% Bis-Tris NuPAGE gel, and stained using the Colloidal Blue Staining Kit (Invitrogen) (*SI Appendix*, Fig. S1*G*). Lanes were subdivided into six slices and mass spectrometry was performed at the Taplin Biological Mass Spectrometry Facility (Harvard Medical School) using an LTQ ion-trap mass spectrometer. In addition to control immunopurifications from the N2 strain, to account for abundant contaminant proteins that bound nonspecifically to the immunopurification matrix, we utilized data from multiple purifications of GFP fusion proteins, which we previously reported (47–49; see *SI Appendix, Materials and Methods* for the details of the filtering criteria used).

Lifespan Analysis. All of the strains were maintained at 20 °C. Ten mid-L4 hermaphrodites were transferred onto NGM plates freshly seeded with OP50-1. These animals were scored for viability every 1 to 3 d, either by movement or tapping them with a platinum wire. The wild-type animals were transferred to NGM plates from the same batch every other day for a week to avoid overcrowding by their progeny. The animals that crawled on the plate sides were censored (*SI Appendix*, Table S2).

Immunostaining. The gonads of day 1 adult hermaphrodites were dissected in egg salt buffer fixed in 1% paraformaldehyde for 5 min and postfixed in cold methanol (–20 °C) for 1 min. Then, the samples were blocked with 1 mg/mL bovine serum albumin (BSA) in 1 × phosphate-buffered saline containing 0.1% Tween 20 (PBT) overnight at 4 °C. Primary antibody incubation was performed in PBT + BSA overnight at 4 °C, while secondary antibody incubation was performed in PBT + BSA for 1.5 to 2 h at room temperature. Gonads were stained with the following antibodies provided by Abby Dernburg, University of California, Berkeley, CA: goat anti-SYP-1 (1:4,000), rabbit anti-ZIM-3 (1:1,000), guinea pig anti-HIM-8 (1:250), and guinea pig anti-HTP-3 (1:300). The guinea pig anti-SUN-1(S8Pi) (1:700) was provided by Verena Jantsch, Max Pertutz Labs, Vienna, Austria, and the rabbit anti-RAD-51 (1:30,000) was provided by Sarit Smolikov, University of Iowa, Iowa City, IA. Secondary antibodies were Cy3-conjugated goat anti-mouse (1:500, Jackson ImmunoResearch), Cy3-conjugated donkey anti-chicken IgY (1:1,000, Jackson ImmunoResearch), and DyLight 488-conjugated donkey anti-guinea pig (1:800, Thermo Fisher Scientific). DAPI was used to detect DNA, and Vectashield (Vector Laboratories) was used as a mounting medium.

Image Acquisition and Processing. Images of day 1 adult hermaphrodites, anesthetized with 0.1% levamisole on 2% agarose pads, were acquired on a Nikon Ti2 inverted microscope equipped with Plan apochromatic aberration correction (Apo) infrared (IR) 60 × and high power (HP) Apo total internal reflection fluorescence 100 × high-magnification oil immersion objective lenses, numerical aperture (NA) 1.27 and 1.49 respectively. Additional details of image acquisition and processing are detailed in *SI Appendix*. To examine the colocalization of SUN-1::mRuby and ZYG-12::GFP, we used Spinning Disk Super Resolution by Optical Pixel Reassignment (SoRA). The 0.30-μm step z-series images were acquired in a Nikon Ti2 inverted microscope equipped with a super-resolution HP plan Apo lambda S 100 × silicon oil immersion objective lens, NA 1.35. Further details of image acquisition and processing are described in *SI Appendix*. The brightness and contrast of the images shown in Fig. 4 were adjusted for presentation identically across all of the strains.

Time-Lapse Acquisition and Processing. Hermaphrodites were selected as mid-L4 larvae and incubated at 20 °C. About 24 h later, young adults were anesthetized in 10 mM levamisole and mounted on 2% agarose pads. Nuclear collapse in the oocytes of *lmn-1* mutants was documented by acquiring 0.4-μm step z-series every 20 s. Extended depth of focus (EDF) projections were created with the NIS Elements software. The movement of SUN-1 foci was documented as previously reported with the following modifications (50): The 0.25-μm step z-series were acquired approximately every 15 s for 6 to 7 min. Maximum intensity projections were made with ImageJ (FIJI), the images were converted to grayscale and their Lookup Tables (LUTs) inverted. Individual SUN-1 foci were followed using StackReg (51) and manual tracking plug-ins. The speed was determined for 84 to 390 individual foci per animal, and the number of animals assessed was equal to or greater than three per strain. All time-lapse images were acquired with the Apo IR 60× water immersion, 1.27 NA objective.

Quantitative and Statistical Analyses. The statistical analyses described below were performed using JMP Pro v14 software (Statistical Discovery, SAS) or Prism 8 (GraphPad Software, LLC.). The statistical analysis details (*n* value, *P* values, confidence intervals, and measures of central tendency) for each experiment are either stated below or in the respective figures, supplemental figures, and figure legends. Kaplan-Meier survival curves followed by Wilcoxon tests were performed for the lifespan data. The Wilcoxon tests of individual pair comparisons for all of the genotypes had a $P < 0.001$, except the *lmn-1(tm1502)* vs. *lmn-1(tm1502); +/mIn1* pair, which had a $P = 0.119$. For the suppression of sterility phenotype data, a contingency analysis of outcome by genotype was performed (*SI Appendix*, Fig. S2*A*). Standard chi square tests were conducted to compare the data from each mutant to those of their respective control [e.g., *lmn-1(–);ooc-5(–)/mIn1* was compared to *lmn-1(–);mIn1*/+]. SUN-1(S8Pi), SUN-1 foci number and speed of movement, and the position of unpaired chromosomes data were tested for equality of group variance. Since they all had unequal variances, nonparametric comparisons were made for each pair using the Wilcoxon method. A one-way ANOVA, followed by Dunnett's comparisons, was performed to analyze the start of the SUN-1(S8Pi) region, using the N2 data as control. The comparison of fluorescence intensity of NPP-12::GFP or GFP::NPP-22 in different subcellular compartments between genetic backgrounds was performed using Prism 8 (GraphPad Software, LLC.). A two-way ANOVA showed that the effect of the different genetic backgrounds was significant, $P < 0.0001$. Bonferroni multiple comparison tests were performed using the fluorescent intensity of the nucleoporins in the otherwise wild-type background as controls. Fig. 4*B* shows the *P* values for these comparisons in the NE.

Data Availability. All data generated in this study are found in the main text or *SI Appendix*. Further information and requests for resources and reagents should be directed to and will be fulfilled by D.G. (green959@umn.edu). We gladly share all *C. elegans* strains generated in this study.

ACKNOWLEDGMENTS. We thank G. W. G. Luxton for encouraging us to pursue this project. We thank A. Dernburg, V. Jantsch, S. Smolikove, D. Starr, and A. Villeneuve for providing antibodies. We thank J. Powers, C. Spike, and T. Starich for comments on the manuscript and encouragement. We thank A. E. Garcia-Vedrenne for guidance on statistics. We thank Nikon Instruments for use of the SoRa microscope. Some strains were provided by the *Caenorhabditis* Genetics Center. This work was supported by NIH (GM57173 and NS095109 to D.G.) and the Dystonia Medical Research Foundation's Barbara Oliver Memorial Dystonia Research Award to G.H.-M.

1. C. Guilluy *et al*., Isolated nuclei adapt to force and reveal a mechanotransduction pathway in the nucleus. *Nat. Cell Biol.* **16**, 376–381 (2014).
2. D. M. Graham, K. Burridge, Mechanotransduction and nuclear function. *Curr. Opin. Cell Biol.* **40**, 98–105 (2016).
3. A. Janin, D. Bauer, F. Ratti, G. Millat, A. Méjat, Nuclear envelopathies: A complex LINC between nuclear envelope and pathology. *Orphanet J. Rare Dis.* **12**, 147 (2017).
4. L. J. Ozelius *et al*., The early-onset torsion dystonia gene (DYT1) encodes an ATP-binding protein. *Nat. Genet.* **17**, 40–48 (1997).
5. A. Kariminejad *et al*., TOR1A variants cause a severe arthrogryposis with developmental delay, strabismus and tremor. *Brain* **140**, 2851–2859 (2017).
6. S. C. Reichert, P. Gonzalez-Alegre, G. H. Scharer, Biallelic *TOR1A* variants in an infant with severe arthrogryposis. *Neurol. Genet.* **3**, e154 (2017).
7. R. E. Goodchild, C. E. Kim, W. T. Dauer, Loss of the dystonia-associated protein torsinA selectively disrupts the neuronal nuclear envelope. *Neuron* **48**, 923–932 (2005).
8. M. J. VanGompel, K. C. Nguyen, D. H. Hall, W. T. Dauer, L. S. Rose, A novel function for the *Caenorhabditis elegans* torsin OOC-5 in nucleoporin localization and nuclear import. *Mol. Biol. Cell* **26**, 1752–1763 (2015).
9. F. C. Nery *et al*., TorsinA binds the KASH domain of nesprins and participates in linkage between nuclear envelope and cytoskeleton. *J. Cell Sci.* **121**, 3476–3486 (2008).
10. C. A. Saunders *et al*., TorsinA controls TAN line assembly and the retrograde flow of dorsal perinuclear actin cables during rearward nuclear movement. *J. Cell Biol.* **216**, 657–674 (2017).
11. J. Hewett *et al*., TorsinA in PC12 cells: Localization in the endoplasmic reticulum and response to stress. *J. Neurosci. Res.* **72**, 158–168 (2003).
12. P. Chen *et al*., The early-onset torsion dystonia-associated protein, torsinA, is a homeostatic regulator of endoplasmic reticulum stress response. *Hum. Mol. Genet.* **19**, 3502–3515 (2010).
13. M. L. Thompson *et al*., TorsinA rescues ER-associated stress and locomotive defects in *C. elegans* models of ALS. *Dis. Model. Mech.* **7**, 233–243 (2014).
14. C. Zhao, R. S. Brown, C. H. Tang, C. C. Hu, C. Schlieker, Site-specific proteolysis mobilizes torsinA from the membrane of the endoplasmic reticulum (ER) in response to ER stress and B cell stimulation. *J. Biol. Chem.* **291**, 9469–9481 (2016).
15. M. Grillet *et al*., Torsins are essential regulators of cellular lipid metabolism. *Dev. Cell* **38**, 235–247 (2016).
16. F. E. Demircioglu *et al*., The AAA + ATPase TorsinA polymerizes into hollow helical tubes with 8.5 subunits per turn. *Nat. Commun.* **10**, 3262 (2019).
17. S. E. Basham, L. S. Rose, Mutations in *ooc-5* and *ooc-3* disrupt oocyte formation and the reestablishment of asymmetric PAR protein localization in two-cell *Caenorhabditis elegans* embryos. *Dev. Biol.* **215**, 253–263 (1999).
18. S. E. Basham, L. S. Rose, The *Caenorhabditis elegans* polarity gene *ooc-5* encodes a Torsin-related protein of the AAA ATPase superfamily. *Development* **128**, 4645–4656 (2001).
19. T. V. Naismith, S. Dalal, P. I. Hanson, Interaction of torsinA with its major binding partners is impaired by the dystonia-associated DeltaGAG deletion. *J. Biol. Chem.* **284**, 27866–27874 (2009).
20. A. E. Rose, R. S. H. Brown, C. Schlieker, Torsins: Not your typical AAA+ ATPases. *Crit. Rev. Biochem. Mol. Biol.* **50**, 532–549 (2015).
21. I. L. Minn, M. M. Rolls, W. Hanna-Rose, C. J. Malone, SUN-1 and ZYG-12, mediators of centrosome-nucleus attachment, are a functional SUN/KASH pair in *Caenorhabditis elegans*. *Mol. Biol. Cell* **20**, 4586–4595 (2009).

22. M. Crisp *et al*., Coupling of the nucleus and cytoplasm: Role of the LINC complex. *J. Cell Biol.* **172**, 41–53 (2006).
23. C. R. Bone, E. C. Tapley, M. Gorjánácz, D. A. Starr, The *Caenorhabditis elegans* SUN protein UNC-84 interacts with lamin to transfer forces from the cytoplasm to the nucleoskeleton during nuclear migration. *Mol. Biol. Cell* **25**, 2853–2865 (2014).
24. J. Liu *et al*., Essential roles for *Caenorhabditis elegans* lamin gene in nuclear organization, cell cycle progression, and spatial organization of nuclear pore complexes. *Mol. Biol. Cell* **11**, 3937–3947 (2000).
25. E. Haithcock *et al*., Age-related changes of nuclear architecture in *Caenorhabditis elegans*. *Proc. Natl. Acad. Sci. U.S.A.* **102**, 16690–16695 (2005).
26. A. Penkner *et al*., The nuclear envelope protein Matefin/SUN-1 is required for homologous pairing in *C. elegans* meiosis. *Dev. Cell* **12**, 873–885 (2007).
27. A. Sato *et al*., Cytoskeletal forces span the nuclear envelope to coordinate meiotic chromosome pairing and synapsis. *Cell* **139**, 907–919 (2009).
28. A. M. Penkner *et al*., Meiotic chromosome homology search involves modifications of the nuclear envelope protein Matefin/SUN-1. *Cell* **139**, 920–933 (2009).
29. O. Rog, A. F. Dernburg, Chromosome pairing and synapsis during *Caenorhabditis elegans* meiosis. *Curr. Opin. Cell Biol.* **25**, 349–356 (2013).
30. A. Woglar *et al*., Matefin/SUN-1 phosphorylation is part of a surveillance mechanism to coordinate chromosome synapsis and recombination with meiotic progression and chromosome movement. *PLoS Genet.* **9**, e1003335 (2013).
31. S. S. Pappas, C. C. Liang, S. Kim, C. O. Rivera, W. T. Dauer, TorsinA dysfunction causes persistent neuronal nuclear pore defects. *Hum. Mol. Genet.* **27**, 407–420 (2018).
32. A. Schetter, P. Askjaer, F. Piano, I. Mattaj, K. Kemphues, Nucleoporins NPP-1, NPP-3, NPP-4, NPP-11 and NPP-13 are required for proper spindle orientation in *C. elegans*. *Dev. Biol.* **289**, 360–371 (2006).
33. N. K. Gill *et al*., DYT1 dystonia patient-derived fibroblasts have increased deformability and susceptibilty to damage by mechanical forces. *Front. Cell Dev. Biol.* **7**, 103 (2019).
34. B. Dominguez Gonzalez *et al*., Excess LINC complexes impair brain morphogenesis in a mouse model of recessive TOR1A disease. *Hum. Mol. Genet.* **27**, 2154–2170 (2018).
35. E. Laudermilch *et al*., Dissecting Torsin/cofactor function at the nuclear envelope: A genetic study. *Mol. Biol. Cell* **27**, 3964–3971 (2016).
36. C. E. Kim, A. Perez, G. Perkins, M. H. Ellisman, W. T. Dauer, A molecular mechanism underlying the neural-specific defect in torsinA mutant mice. *Proc. Natl. Acad. Sci. U.S.A.* **107**, 9861–9866 (2010).
37. U. Zabel *et al*., Nic96p is required for nuclear pore formation and functionally interacts with a novel nucleoporin, Nup188p. *J. Cell Biol.* **133**, 1141–1152 (1996).
38. S. R. Wente, G. Blobel, A temperature-sensitive NUP116 null mutant forms a nuclear envelope seal over the yeast nuclear pore complex thereby blocking nucleocytoplasmic traffic. *J. Cell Biol.* **123**, 275–284 (1993).
39. Q. Liu *et al*., Functional association of Sun1 with nuclear pore complexes. *J. Cell Biol.* **178**, 785–798 (2007).
40. P. H. Kim *et al*., Disrupting the LINC complex in smooth muscle cells reduces aortic disease in a mouse model of Hutchinson-Gilford progeria syndrome. *Sci. Transl. Med.* **10**, eaat7163 (2018).
41. C. Y. Chen *et al*., Accumulation of the inner nuclear envelope protein Sun1 is pathogenic in progeric and dystrophic laminopathies. *Cell* **149**, 565–577 (2012).
42. J.-Y. Wang *et al*., Sun1 deficiency leads to cerebellar ataxia in mice. *Dis. Model. Mech.* **8**, 957–967 (2015).
43. J. A. Arribere *et al*., Efficient marker-free recovery of custom genetic modifications with CRISPR/Cas9 in *Caenorhabditis elegans*. *Genetics* **198**, 837–846 (2014).
44. D. J. Dickinson, J. D. Ward, D. J. Reiner, B. Goldstein, Engineering the *Caenorhabditis elegans* genome using Cas9-triggered homologous recombination. *Nat. Methods* **10**, 1028–1034 (2013).
45. A. Paix *et al*., Scalable and versatile genome editing using linear DNAs with microhomology to Cas9 sites in *Caenorhabditis elegans*. *Genetics* **198**, 1347–1356 (2014).
46. D. J. Dickinson, A. M. Pani, J. K. Heppert, C. D. Higgins, B. Goldstein, Streamlined genome engineering with a self-excising drug selection cassette. *Genetics* **200**, 1035–1049 (2015).
47. C. A. Spike *et al*., Translational control of the oogenic program by components of OMA ribonucleoprotein particles in *Caenorhabditis elegans*. *Genetics* **198**, 1513–1533 (2014).
48. T. Tsukamoto *et al*., LIN-41 and OMA ribonucleoprotein complexes mediate a translational repression-to-activation switch controlling oocyte meiotic maturation and the oocyte-to-embryo transition in *Caenorhabditis elegans*. *Genetics* **206**, 2007–2039 (2017).
49. T. Tsukamoto *et al*., Insights into the involvement of spliceosomal mutations in myelodysplastic disorders from analysis of SACY-1/DDX41 in *Caenorhabditis elegans*. *Genetics* **214**, 869–893 (2020).
50. A. Baudrimont *et al*., Leptotene/zygotene chromosome movement via the SUN/KASH protein bridge in *Caenorhabditis elegans*. *PLoS Genet.* **6**, e1001219 (2010).
51. P. Thévenaz, U. E. Ruttimann, M. Unser, A pyramid approach to subpixel registration based on intensity. *IEEE Trans. Image Process.* **7**, 27–41 (1998).